Rev. Roum. Sci. Techn.– Électrotechn. et Énerg.
Vol. **69**, *3*, pp. 359–364, Bucarest, 2024

Génie biomédical
Biomedical Engineering

MEG AND PET IMAGES-BASED BRAIN TUMOR DETECTION USING KAPUR'S OTSU SEGMENTATION AND SOOTY OPTIMIZED MOBILENET CLASSIFICATION

AHILAN APPATHURAI[1], ANLIN SAHAYA INFANT TINU [2], MUTHUKUMARAN NARAYANAPERUMAL[3]

Keywords: Brain tumor detection; Hybrid hexagonal features Magnetoencephalography (MEG) and positron emission tomography (PET) images; Deep learning; Kapur's Otsu threshold algorithm; Sooty optimization-based MobileNet.

Deep learning techniques have revolutionized medical image analysis recently, particularly in brain tumor (BT) detection. A comprehensive overview of the advancements and challenges associated with employing deep learning methodologies for the accurate and timely detection of BT. This work proposes a novel brain hybrid hexagonal mobile network (BH^{2}Mnet) to identify benign and malignant tumors using MEG and PET images. An adaptive bilateral filter (ABF) is used as a de-noising for input images to eliminate noise artifacts. Eliminating the skull and outer cortical regions, a process known as "skull stripping" is utilized to enhance the number of training images. The de-noised images are segmented to detect the BT using Kapur's Otsu threshold (KOT) algorithm. Based on these segmented tumors, hexagonal feature sets with and without segmentation masks are produced using hybrid hexagonal features (HHF). Finally, the Sooty optimization-based MobileNet classifier is employed to classify the BT into benign, malignant cases. It was determined that the proposed BH^{2}Mnet approach was 99.21% accurate in classifying data. According to the proposed BH^{2}Mnet NS-CNN, the total accuracy is enhanced by 1.67%, 2.69%, and 4.11% compared to hybrid DAE, BFC, Deep CNN, and Neutrosophy.

1. INTRODUCTION

Brain tumors (BT) are caused by unrestrained cell growth. If these cells are not identified early, they can lead to mortality when they proliferate out of control in a particular area of the brain [1,2]. It is considered one of the worst illnesses in the globe due to its growing impact and high death rate in all age categories [3]. In India, it is the second most significant cause of cancer. According to the most recent estimate by the American Cancer Society, 24,000 Americans will receive a brain cancer diagnosis in 2020, and 19,000 more people will die from brain tumors because of the increased use of technology such as smartphones and tablets [4]. Brain anomalies have long been detected using medical imaging techniques, including PET, CT, MRI, and MEG [5,6]. Brain tumors can cause headaches, seizures, personality changes, and even loss of motor function or speech impairment, depending on where the tumor is located. Brain tumors can also cause other complications, such as hydrocephalus, increased intracranial pressure, and cerebral edema [7].

The abnormal modification of brain cells causes gliomas, which are prevalent malignant brain tumors [8,9]. Surgery is necessary because of the intricacy of the HGG development, which has significantly deteriorated and is believed to be a malignant tumor. Although patients' lives are not affected considerably by LGG, their lives are lengthened during treatment [10,11].

Due to the rapid development of intense medical imaging modalities, such as modern MRI scanners, and the volume of data generated, more automated techniques are needed in computer-aided diagnosis [12,13]. Clinicians must spend much time and effort looking for anomalies in various complex medical imaging [14]. Technology that can automatically detect organs and any possible anomalies in them is thus required, as well as technology that can offer valuable measurements [15].

The MRI and CT [16] images were analyzed using supervised learning SVM classifiers. The existing body of research comprehensively comprehends the image analysis process [17]. The incapacity of the MRI to differentiate between benign and malignant tumors might occasionally result in false positive results. To overcome this problem, a novel brain hybrid hexagonal mobile network (BH^{2}Mnet) is proposed to identify the tumors using MEG and PET images. The critical contribution of the proposed BH^{2}Mnet is summarized as follows,

- The gathered MEG and PET images are denoised using the ABF to eliminate the noise artifacts. The outer cortex and skull region are removed using the skull stripping technique, which will be implemented to raise the volume of the training datasets.
- The KOT algorithm segments the pre-processed images to identify the brain tumor.
- Based on these segmented tumors, hexagonal feature sets with and without segmentation masks are produced using HHF.
- Finally, the sooty optimization-based MobileNet classifier is employed to classify the tumors into benign, malignant cases.

The remaining components of this investigation were divided into the following five categories: section 2 reviews the relevant works, section 3 introduces the suggested BH2Mnet approach, section 4 gives the findings and discussion, and section 5 concludes with suggestions for further research.

2. LITERATURE SURVEY

This article presents an overview of related works on applying deep learning (DL) techniques to brain tumor disease identification. Recently, more methods have been used to detect various brain diseases. This section briefly explains brain tumor detection using multiple images.

[1] PSN College of Engineering and Technology, Tirunelveli, India
[2] Anna University, Chennai, India. Correspondence address
[3] Sri Eshwar College of Engineering, Coimbatore, India
Emails: akhilanappathurai@psncet.ac.in, anlin@psncet.ac.in (correspondence), muthukumaran.n@sece.ac.in

DOI: 10.59277/RRST-EE.2024.69.3.18

With its high cost and maintenance requirements, magnetoencephalography (MEG) has limited applicability [18], even though numerous studies have shown it to be accurate in localizing major BT in patient populations. A database search was utilized to locate the results that employed both approaches to perform pre-operative assessments on BT patients.

[19] detected cerebral tumors using MR images through a combination of random forest classification and the application of a median filter. A median filter is proposed to improve skull stripping in MRI images.

[20] investigated using a hybrid segmentation approach combining DAE and BFC to classify brain tumors. This method effectively categorizes brain MR images using DAE, JOA, and SoftMax regression.

[21] a deep CNN with a multiscale approach was used to propose a completely automatic BT classification and segmentation method. The neural method proposed here can analyze MRI scans with gliomas, meningiomas, and pituitary tumors in sagittal, coronal, and axial views without removing the skull and vertebral column from the input images.

[22] introduced a transfer learning model and trained multiple deep CNNs to extract intricate features from brain MRIs. Among various machine learning classifiers, SVM with RBF kernel performs better in diagnosing BT using MRI data.

[23] provided a hybrid strategy using neutrosophy and convolutional neural networks (NS-CNN). MRI data was divided using the NS-EMFSE (neutrophic set – expert maximum fuzzy-sure entropy) method.

[24] recommended using noninvasive magnetic resonance imaging to grade brain cancers. Using the perspectives of five DL models and five ML models, the suggested DL and ML-based majority voting (MajVot) ensemble algorithms enhanced the classification performance of four clinically significant BT images.

[25] proposed the SEResU-Net multimodal BT segmentation technique. SEResU-Net is an improved version of U-Net that combines the squeeze-and-excitation network with the deep left-over network. The SEResU-Net mean dice comparison coefficients for the whole tumor, the tumor core, and the amplified BT were, respectively, 0.9373, 0.8758, and 0.9108.

The existing method for brain tumor detection utilizes MRI images. Still, small-size tumors will not be identified, and one cannot yet evaluate the presence of an altered blood-brain [29–32]. The technologies are well-matched, but only MEG provides spatial and temporal information about brain activity.

3. BRAIN HYBRID HEXAGONAL MOBILE NETWORK METHODOLOGY

The research proposes a novel Brain Hybrid Hexagonal Mobile Network (BH^{2}Mnet) for identifying benign and malignant tumors. The de-noised images are segmented using the KOT algorithm to identify the BT. HHF creates hexagonal feature sets based on these segmented tumors with and without segmentation masks. Finally, the Sooty optimization-based MobileNet classifier is employed to classify the BT into benign and malignant cases. Figure 1 illustrates the general process flow for the proposed BH^{2}Mnet.

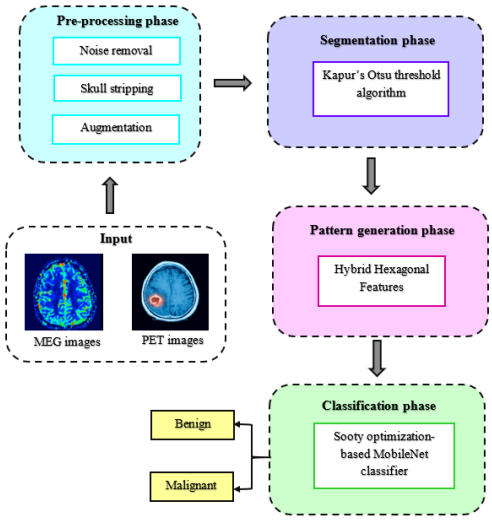

Fig. 1 – The general process workflow of the proposed BH^{2}Mnet.

3.1. DATASET DESCRIPTION

The first folder in Kaggle's dataset [26] has 1 500 MEG scans showing a brain tumor; the second folder has 1 500 MEG scans of healthy brains; and the third folder has some unlabelled MEG images for testing. The latter folder is not utilized because an alternative method for handling the test data is being considered. Therefore, the final database produced is predicated on the initial two files and has 3 000 images dispersed as input data in the following manner: 1 500 images with tumors and 1500 without them. We split the dataset into 80% training and 20% testing. In addition, 10% of the training dataset was used for validation during the training phase.

3.2. ADAPTIVE BILATERAL FILTER

MEG and PET images have been de-noised utilizing an ABF to eliminate noise artifacts. The authors present the ABF, a novel method for enhancing and refining images in this context. Utilizing previously defined terms such as $[u_s, v_s]$ and Ω_{u_s,v_s}, and considering the normalization factor, the proposed shift-variant ABF's reaction at $[u_s, v_s]$ to an impulse at $[u,v]$ is outlined at the bottom of the page

$$r_{u_s v_s} = \sum_{u=u_s-N}^{u_s+N} \sum_{v=v_s-N}^{v_s+N} \exp\left(-\frac{(u-u_s)^2+(v-v_s)^2}{2\sigma_{d^2}}\right) \times$$

$$\times \exp\left(-\frac{(g[u,v]-g[u_s,v_s]-\zeta[u_s,v_s])^2}{2\sigma_{r\cdot 2}[u_s,v_s]}\right). \quad (1)$$

ABF preserves the fundamental design of a bilateral filter while incorporating two notable changes. The offset ζ is first applied to the filter in the ABF. Secondly, the locally adjustable parameters of the ABF comprise the filter's μ and width. A fixed low-pass Gaussian domain filter is the ABF. In the case of fixed r, the ABF becomes a conventional bilateral filter. ABF uses a fixed low-pass Gaussian filter as its domain filter.

The initial threshold value is estimated by utilizing the following equation, which accounts for the intensities b_y and b_z of pixels k_p and k_q

$$\mathrm{MS} = \mathrm{V} \times \sum_{k=0}^{255} \frac{b_y+b_z}{2}. \quad (2)$$

The Laplacian second-order differential equation, denoted by V, distributes pixels uniformly throughout the blood smear images. The process for computing V is

$$V = \frac{\partial^2 V}{\partial k_p} + \frac{\partial^2 V}{\partial k_q}. \quad (3)$$

These processed images are augmented using common strategies (flip, flop, zoom, and so on) to enhance the no. of images in the training set.

3.3. DATA AUGMENTATION

A limited number of datasets are provided for the group tests, so deep learning algorithms cannot create a deep system from these datasets. Figure 2 shows the sample images of data augmentation. The multi-level expansion approach enables our deep system to handle missing datasets and requires fewer calculation parameters, speeding up the preparation process. The image should first be supplied as a pair of two-dimensional vectors. To find the magnitude and angle of a two-dimensional vector ($x(J)$, $y(J)$),

$$\text{Magnitude } (J) = \sqrt{x(J)^2 + y(J)^2}, \quad (4)$$

$$\text{Angle } (J) = \text{atan2}(y(J), x(J)) \, [180/\pi]. \quad (5)$$

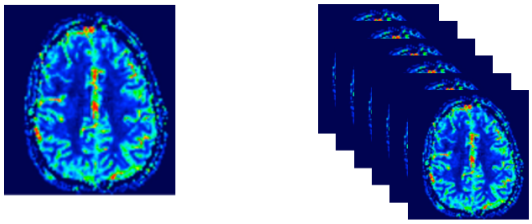

Fig. 2 – The sample images of data augmentation.

After that, the brain tumor for each sample will be computed so that our deep network can quickly extract the low-level properties.

3.4. KAPUR'S OTSU THRESHOLD ALGORITHM

The Otsu threshold method developed by Kapur is used to separate the brain tumor from the denoised images. An overview of Kapur's original Otsu threshold algorithm is given in this section. In multi-level segmentation, Kapur's method can be a valuable metric. In 1985, Kapur developed an entropy technique to determine the optimal threshold values for segmented classes, which maximized their entropy histograms. The entropy presented by Shannon is:

$$H = -\sum_{n=1}^{m} p_k \log(p_k), \quad (6)$$

where m is the entire no. of levels in the grey image, H is the entropy, and p_k is the probability of the nth grey level. This analysis considers the probability distribution between an image's foreground and background. Considering the distribution of probability for a grey level image to be p_1, p_2, p_3,...,p. They are defined as follows:

$$A: \frac{p_1}{p_s}\frac{p_2}{p_s} \dots\dots\dots\dots\dots\dots \frac{p_s}{p_s},$$

$$B: \frac{p_{s+1}}{1-p_s}\frac{p_{s+2}}{1-p_s} \dots\dots\dots\dots\dots\dots \frac{p_n}{1-p_s}.$$

H(A) and H(B) in eqs. (9) and (10) give the entropies associated with A and B. (9) and (10), respectively To extract the maximum amount of information between the background and foreground, the sum of H(A) and H(B) must equal ϕ_s

$$H(A) = \text{In}p_s + \frac{H_i}{p_s}, \quad (7)$$

$$H(B) = -\sum_{i=1}^{s} \frac{p_i}{p_s} \text{In}\frac{p_i}{1-p_s} \text{In}\frac{p_i}{1-p_s}, \quad (8)$$

$$H(B) = \text{In}\,(1-p_s)\frac{H_n - H_s}{1-p_s}, \quad (8)$$

$$\phi_s = H_A + H_B = \text{In}p_s + \frac{H_s}{P_s} + \text{In}\,(1-P_s) + \frac{H_n - H_s}{1-p_s}, \quad (9)$$

$$\phi_s = \text{In}p_s + \frac{(H_n - H_s)p_s + H_s(1-p_s)}{p_s(1-p_s)}. \quad (10)$$

Equation (10) of ϕ_s yields the threshold value, which is the maximum when the discrete values of s in the equation are considered.

3.5. HYBRID HEXAGONAL FEATURES

In this section, hybrid hexagonal features were briefly explained. The segmented region produced by the output of Kapur's Otsu threshold method is used as an input for the hybrid hexagonal features (HHF), which creates new hexagonal features from the input. Visible characteristics like the look and various seized intensity level variations determine the texture qualities of digital images. Visible characteristics like the look and various seized intensity level variations determine the texture qualities of digital images. HHF is suggested to enhance the system's performance by recognizing the textural characteristics of the segmented tumor with hexagonal features. The HHF algorithm is suggested to boost system performance. In Fig. 3, a clockwise selection of a hexagonal feature of pixel values is demonstrated.

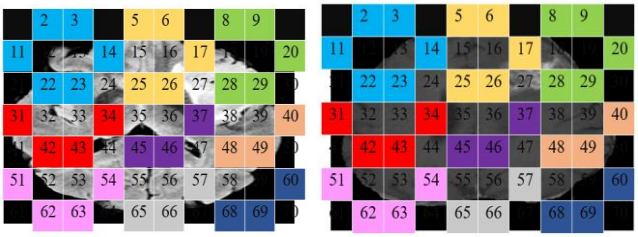

Fig. 3 – An example of selecting pixels for a hexagonal feature.

The altered bits are subjected to an XOR operation to obtain the partial bits. Three channels can be obtained using an OR operation on the incomplete bits. 64 patterns are possible as each channel contains six bits. The neighboring top pixel, with a value of 32, is surrounded by eight neighboring pixels. Among these neighbors, the five adjacent to it are highlighted in orange. The surrounding right pixel, which contains five adjacent pixels shown in blue, also has a value of 42.

3.6. SOOTY OPTIMIZATION-BASED MOBILE NET (MN) CLASSIFIER

The Sooty tern optimization-based MobileNet classifier is employed to classify the tumors into benign, malignant cases. Then, Sooty tern optimization is used to improve the performance of the MobileNet classification.

In [27], the Sooty tern optimization (STO) algorithm was introduced. The sooty tern bird's aggressive behavior served as the algorithm's inspiration. Sooty terns typically live in colonies. To find and attack a target, they use their intelligence. Sooty terns are most known for their migrating and attacking habits. The information that follows sheds light on sooty tern birds:

- During migration, sooty terns migrate in groups. The starting locations of sooty terns differ to prevent collisions.
- Sooty terns with different fitness levels within a group can still cover the same distance as the most fit individuals.
- The fittest sooty tern, sooty terns with lower fitness levels, can improve their initial locations.

Depth-wise separable convolutions (DWSC), the

foundation of MobileNet [28], consist of two main layers: pointwise and depth-wise convolutions. Figure 4 displays the MobileNet-enabled hybrid hexagonal feature pattern.

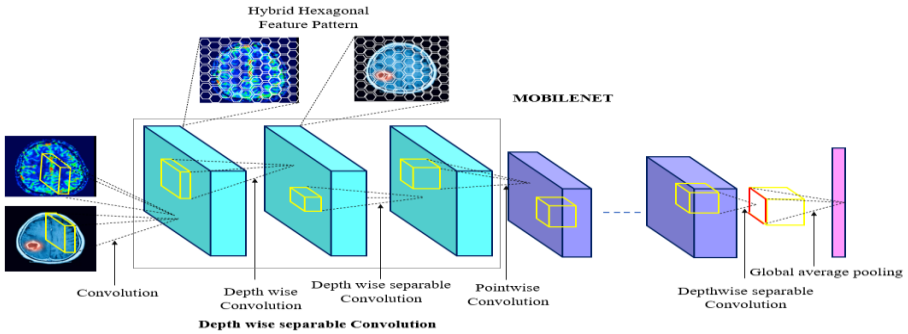

Fig. 4 – Hybrid Hexagonal Feature Pattern with MN.

Table 1 illustrates the architecture of MN, which includes the following layers: global average pooling layer, reshape layer, dropout layer, convolutional layer, SoftMax layer, and reshape layer.

Table 1

architecture of MobileNet

MobileNet
Input Layer
Convolution Layer
Depth wise *n* convolution layer batch normalization
ReLU
+
Pointwise *n* coevolution layer
Batchwise normalization
ReLU
(*n*=1, 2, 3,……13 layers)
Global Average Pooling Layer
Reshape layer
Dropout layer
Convolutional layer
SoftMax layer
Reshape Layer
Output

The DWSC is described by the BN and ReLU layers. The four million parameters in this model are incredibly small compared to other models.

4. RESULT AND DISCUSSION

This experimental design used MATLAB 2019b, a deep learning toolkit. This outcome research used multimodality for pre-processing medical imaging, such as MEG and PET scans, from the publicly available Kaggle dataset.

4.1. PERFORMANCE ANALYSIS

This study utilizes precision (PRE), specificity (SPE), accuracy (ACC), sensitivity (SEN), and F1 scores for conducting performance analysis.

$$specficity = \frac{TN}{TN+FP}, \quad (11)$$

$$Recall = \frac{TP}{TP+FN}, \quad (12)$$

$$Accuracy = \frac{TP+TN}{TP+TN+FP+FN}, \quad (13)$$

$$Precision = \frac{TP}{TP+FP}, \quad (14)$$

$$f1 = 2\left(\frac{precision*recall}{precision+recall}\right). \quad (15)$$

where *FN*, *FP*, *TN*, and *TP* designate the false negative, false positive, true negative, and true positive.

Table 2 shows the classification of BT detection classes according to particular characteristics. Figure 6 compares the BH^{2}Mnet model's performance for benign and malignant tumors. BH^{2}Mnet is predicted to have an accuracy between 99.81% and 98.36%.

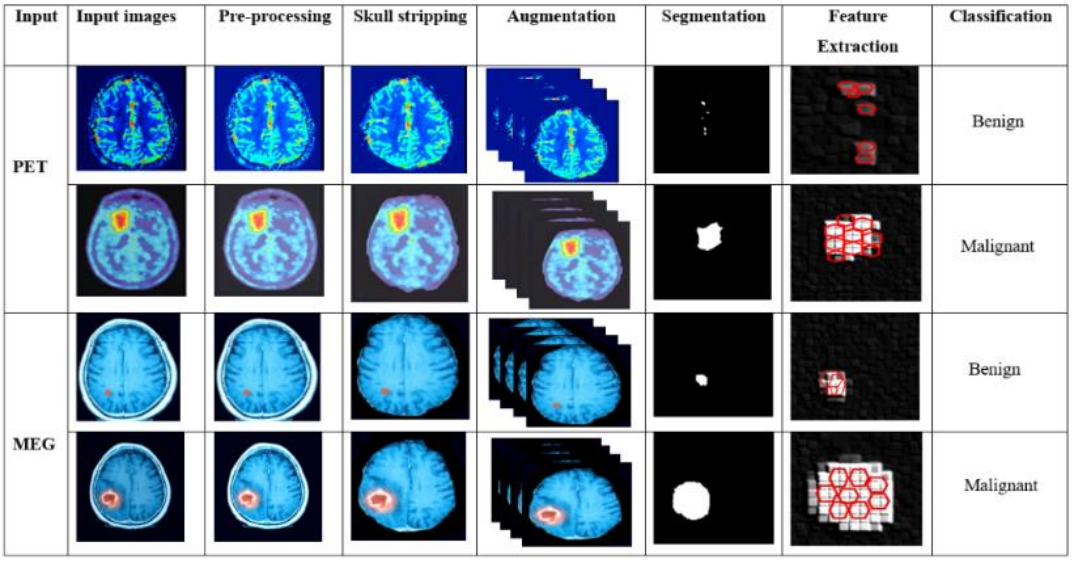

Fig. 5 – The simulation results of the proposed Brain Hybrid Hexagonal Mobile Network (BH^{2}Mnet).

Figure 5 shows the simulation results of the BH^{2}Mnet visualization. Column 1 comprises the inputs MEG and PET, whereas column 2 is a collection of input images of brain tumors obtained from MEG and PET images. Then, images

are denoised using an adaptive bilateral filter to remove noise artifacts (column 3). Skull stripping is then used in column 4 to remove the outer cortex and skull region, and column 5 contains the augmented images. Column 6 displays the KOT algorithm with segmented images. In column 7, HHF creates hexagonal feature sets with and without segmentation masks. Column 8 displays the classification outcomes.

Table 2

Classification	Accuracy	Specificity	Sensitivity	Precision	F1score
Benign	99.81	95.62	94.21	94.22	94.56
Malignant	98.36	93.71	95.63	92.06	97.05

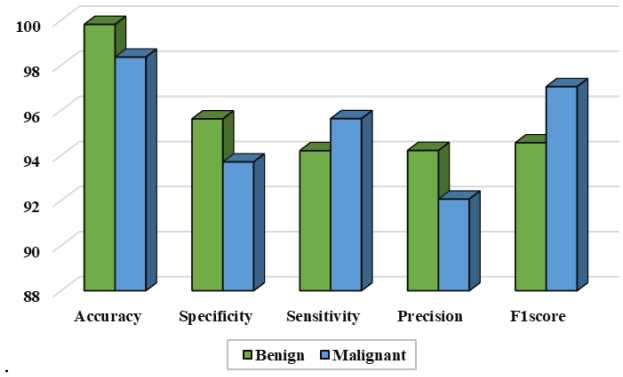

Fig. 6 – Metrics for two types of performance.

Table 3

Performance analysis of the proposed BH²Mnet

Images		Parameters				
MEG	PET	ACC	SPE	PRE	REC	F1 score
M1	P1	99.03	97.26	95.35	90.85	97.46
M2	P2	98.54	95.72	92.46	92.19	97.57
M3	P3	**99.72**	**98.16**	**98.53**	**99.24**	**97.91**
M4	P4	95.41	97.30	89.25	98.48	96.48
M5	P5	99.15	98.01	97.57	89.56	94.56

Table 3 shows the performance of the proposed BH2Mnet for gathered Kaggle dataset sample images of MEG and PET. The efficiency of the proposed method was evaluated using the gathered Kaggle dataset, and image 3 attained a high level of accuracy in classifying brain disease.

The Proposed BH²Mnet approach has acquired high accuracy in training and validation accuracy and loss graph, as shown in Fig. 7.

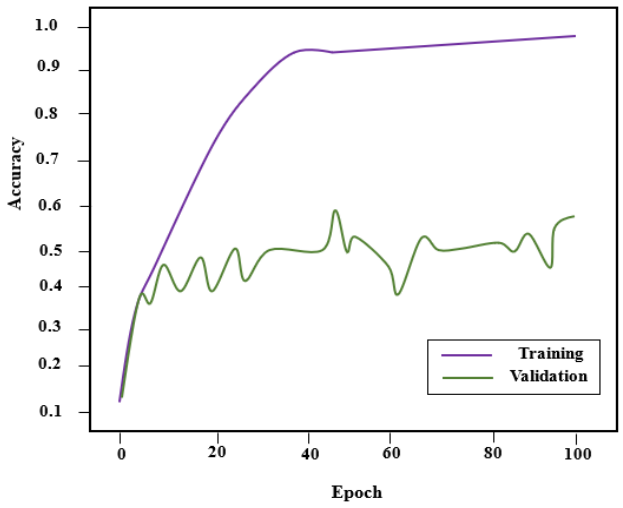

a) Accuracy curve

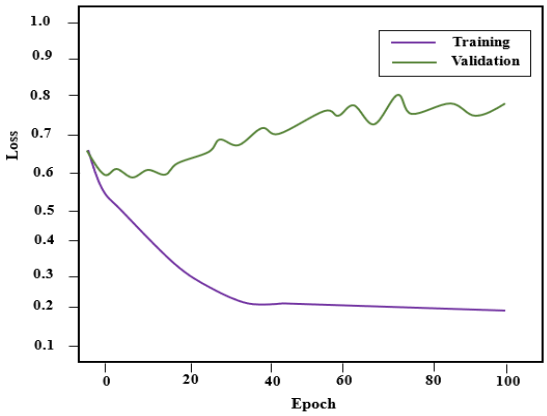

b) Loss curve

Fig. 7 – ACC and loss curves of the proposed brain hybrid hexagonal mobile network (BH²Mnet).

4.2. COMPARATIVE ANALYSIS

The efficacy of existing techniques was examined to show that the proposed strategy produces more effective results. The proposed model predicts performance based on specificity and sensitivity, with an accuracy range of 99.07%.

Table 4 indicates that conventional networks such as CNN, Resnet, AlexNet, and MobileNet require more complexity to achieve high accuracy. With fewer constraints, MobileNet reduces complexity while preserving a high accuracy range of 99.21%.

Table 4

Comparison of state-of-the-art DL networks with BH²Mnet networks

Techniques	ACC	SPE	PRE	REC	F1score
CNN	93.05%	91.34%	92.44%	89.25%	90.79%
Resnet	94.17%	92.72%	93.35%	90.41%	93.83%
AlexNet	96.85%	93.86%	94.04%	92.08%	95.37%
MobileNet	99.21%	96.90%	98.95%	95.42%	97.88%

The BH²Mnet enhanced the ACC by 1.67%, 2.69%, and 4.11%, which is better than hybrid DAE and BFC, Deep CNN, and (NS-CNN), respectively. According to the comparison above, the BH2Mnet model outperforms state-of-the-art models in accuracy.

Table 5

A comparative analysis of the current and proposed models

Authors	Methods	Accuracy
Raja, P.S., [19]	hybrid DAE and BFC	98.05%
Díaz-Pernas, [20]	Deep CNN	97.03%
Özyurt, F., [22]	Neutrosophy, CNN (NS-CNN)	95.62%
Proposed	**Brain Hybrid Hexagonal Mobile Network (BH²Mnet)**	**99.72%**

Table 5 demonstrates that the recommended method is more accurate than conventional networks such as hybrid DAE, BFC, Deep CNN, and NS-CNN. At 99.54%, the projected Brain Hybrid Hexagonal Mobile Network (BH²Mnet) retains exceptional accuracy levels.

5. CONCLUSIONS

Researchers have developed a novel BH²Mnet to differentiate benign from malignant tumors based on the MEG and PET images. The input images are pre-processed using ABF to remove noise artifacts. The BT is separated from the previously processed images using Kapur's Otsu threshold technique. Finally, the Sooty optimization-based MobileNet classifier is employed to classify the BT into benign,

malignant cases. The classification ACC of the proposed BH²Mnet was 99.21%, respectively. The Proposed BH²Mnet enhances the total ACC by 1.67%, 2.69%, and 4.11%, improved than hybrid DAE, BFC, Deep CNN, and NS-CNN. We plan to increase training and testing datasets for the accurate detection of BT diseases in the future.

Received on 3 August 2023

REFERENCES

1. A. Hossain, M.T. Islam, S.K. Abdul Rahim, M.A. Rahman, T. Rahman, H. Arshad, A. Khandakar, M.A. Ayari, M.E. Chowdhury, *A lightweight deep learning based microwave brain image network model for brain tumor classification using reconstructed microwave brain (RMB) images*, Biosensors, **13**, *2*, pp. 238 (2023).
2. R. Sundarasekar, A. Appathurai, *Efficient brain tumor detection and classification using magnetic resonance imaging*, Biomedical Physics & Engineering Express, **7**, *5*, 055007 (2021).
3. M.K. Islam, M.S. Ali, M.S. Miah, M.M. Rahman, M.S. Alam, M.A. Hossain, *Brain tumor detection in MR image using superpixels, principal component analysis and template-based K-means clustering algorithm*, Machine Learning with Applications, **5**, 100044 (2021).
4. E. Porumb-Andrese, C.F. Costea, G. Macovei, G.F. Dumitrescu, L.A. Blaj, I. Prutianu, A.I. Cucu, *Humps and bumps of head: review of meningiomas of the scalp*, Romanian Journal of Morphology and Embryology, **64**, *4*, pp. 467–473 (2023).
5. S. Hussain, I. Mubeen, N. Ullah, S.S.U.D. Shah, B.A. Khan, M. Zahoor, M.A. Sultan, *Modern diagnostic imaging technique applications and risk factors in the medical field: a review*, BioMed Research International, 2022.
6. A.V. Reddy, P.K. Mallick, B. Srinivasa Rao, P. Kanakamedala, *An efficient brain tumor classification using MRI images with hybrid deep intelligence model*, The Imaging Science Journal, 1–15 (2023).
7. M.B. Coomans, S.D. van der Linden, K. Gehring, M.J. Taphoorn, *Treatment of cognitive deficits in brain tumour patients: current status and future directions*, Current Opinion in Oncology, **31**, *6*, pp. 540 (2019).
8. A.I. Cucu, C.F. Costea, G. Macovei, G.F. Dumitrescu, A. Sava, L.A. Blaj, I. Prutianu, E. Porumb-Andrese, C.G. Dascălu, M. Coşman, I. Poeată, *Clinicopathological characteristics and prognostic factors of atypical meningiomas with bone invasion: a retrospective analysis of nine cases and literature review*, Romanian Journal of Morphology and Embryology, **64**, *4*, pp. 509–515 (2023).
9. S. Li, C. Wang, J. Chen, Y. Lan, W. Zhang, Z. Kang, Y. Zheng, R. Zhang, J. Yu, W. Li, *Signaling pathways in brain tumors and therapeutic interventions*, Signal Transduction and Targeted Therapy, **8**, *1*, p. 8 (2023).
10. A. Ramaiah, P.D. Balasubramanian, A. Appathurai, N.A. Muthukumaran, *Detection of Parkinson's disease via Clifford gradient-based recurrent neural network using multi-dimensional data*, Rev. Roum. Sci. Techn. – Électrotechn. et Énerg., **69**, *1*, pp. 103–108 (2024).
11. V.V.S. Sasank, S. Venkateswarlu, *Hybridized deep neural network using adaptive rain optimizer algorithm for multi-grade brain tumor classification of MRI images*, Digital Technologies Research and Applications, **1**, *1*, pp. 14–31 (2022).
12. K.S. Rahul, *Hybrid Model Implementation for Brain Tumor Detection System using Deep Neural Networks*, International Journal for Research in Applied Science & Engineering Technology (IJRASET), **8**, *12*, pp. 281–285 (2020).
13. D.P. Kruti, *Medical image processing*, IJSCUB, **12**, *4*, pp. 646–652 (2022).
14. G.G. Tolun, Y.A. Kaplan, *Development of backpropagation algorithm for estimating solar radiation: a case study in Turkey*, Rev. Roum. Sci. Techn. – Électrotechn. et Énerg., **68**, *3*, pp. 313–316 (2023).
15. S.K. Zhou, H. Greenspan, C. Davatzikos, J.S. Duncan, B. van Ginneken, A. Madabhushi, R.M. Summers, *A review of deep learning in medical imaging: Imaging traits, technology trends, case studies with progress highlights, and future promises*, Proceedings of the IEEE, **109**, *5*, pp. 820–838 (2021).
16. A. Topor, D. Ulieru, C. Ravariu, F. Babarada, *Development of a new one-eye implant by 3D bioprinting technique*, Rev. Roum. Sci. Techn. – Électrotechn. et Énerg., **68**, *2*, pp. 247–250 (2023).
17. M.A. Khan, I. Ashraf, M. Alhaisoni, R. Damaševičius, R. Scherer, A. Rehman, S.A.C. Bukhari, *Multimodal brain tumor classification using deep learning and robust feature selection: a machine learning application for radiologists*, Diagnostics, **10**, *8*, pp. 565 (2020).
18. E. Cargnelutti, B. Tomasino, *Pre-operative functional mapping in patients with brain tumors by fMRI and MEG: advantages and disadvantages in the use of one technique over the other*, Life, **13**, *3*, p. 609 (2023).
19. M. Thayumanavan, A. Ramasamy, *An efficient approach for brain tumor detection and segmentation in MR brain images using random forest classifier*, Concurrent Eng., **29**, *3*, pp. 266–274 (2021).
20. P.S. Raja, *Brain tumor classification using a hybrid deep autoencoder with Bayesian fuzzy clustering-based segmentation approach*, Biocybern. Biomed. Eng., **40**, *1*, pp. 440–453 (2020).
21. F.J. Díaz-Pernas, M. Martínez-Zarzuela, M. Antón-Rodríguez, D. González-Ortega, *A deep learning approach for brain tumor classification and segmentation using a multiscale convolutional neural network*, Healthcare, **9**, *2*, p. 153 (2021).
22. J. Kang, Z. Ullah, J. Gwak, *MRI-based brain tumor classification using ensemble of deep features and machine learning classifiers*, Sens, **21**, *6*, p. 2222 (2021).
23. F. Özyurt, E. Sert, E. Avci, E. Dogantekin, *Brain tumor detection based on convolutional neural network with neutrosophic expert maximum fuzzy sure entropy*, Measurement, **147**, 106830 (2019).
24. G.S. Tandel, A. Tiwari, O.G. Kakde, *Performance optimisation of deep learning models using majority voting algorithm for brain tumour classification*, Comput. Biol. Med., **135**, p. 104564 (2021).
25. C. Yan, J. Ding, H. Zhang, K. Tong, B. Hua, S. Shi, *SEResU-Net for Multimodal Brain Tumor Segmentation*, IEEE Access, **10**, pp. 117033–117044 (2022).
26. S. Kuraparthi, M.K. Reddy, C.N. Sujatha, H. Valiveti, C. Duggineni, M. Kollati, P. Kora, *Brain tumor classification of MRI images using deep convolutional neural network*, Traitement du Signal, **38**, *4*, pp. 1171–1179 (2021).
27. A. Singh, A. Sharma, S. Rajput, A.K. Mondal, A. Bose, M. Ram, *Parameter extraction of solar module using the sooty tern optimization algorithm*, Electronics, **11**, *4*, p. 564 (2022).
28. T.H. Arfan, M. Hayaty, A. Hadinegoro, *Classification of brain tumours types based on MRI images using MobileNet*, 2nd International Conference on Innovative and Creative Information Technology (ICITech) IEEE, pp. 69–73 (2021).
29. L.J. Ahmed, P.M. Bruntha, S. Dhanasekar, V. Chitra, D. Balaji, N. Senathipathi, *An improvised image registration technique for brain tumor identification and segmentation using ANN Approach*, 6th International Conference on Devices, Circuits and Systems (ICDCS), IEEE, pp. 80–84 (2022).
30. S. Gnana Sophia, K.K. Thanammal, S.S. Sujatha, *Secure storage of lung brain multi-modal medical images using DNA homomorphic encryption*, International Journal of Current Bio-Medical Engineering, **1**, *1*, pp. 16–22 (2023).
31. S. Karpakam, N. Senthilkumar, R. Kishorekumar, U. Ramani, P. Malini, S. Irfanbasha, *Investigation of brain tumor recognition and classification using deep learning in medical image processing*, International Conference on Augmented Intelligence and Sustainable Systems (ICAISS), IEEE, pp. 185–188 (2022).
32. A. Jegatheesh, N. Kopperundevi, M.A.A.S.I. Tinu, *Brain aneurysm detection via firefly optimized spiking neural network*, International Journal of Current Bio-Medical Engineering, **1**, *1*, pp. 23–29 (2023).